Acceleration-driven dynamics of Josephson vortices in coplanar superfluid rings

Yurii Borysenko,[1] Nataliia Bazhan,[2] Olena Prykhodko,[1] Dominik Pfeiffer,[3] Ludwig Lind,[3] Gerhard Birkl,[3,4] and Alexander Yakimenko[1,5]

[1]*Department of Physics, Taras Shevchenko National University of Kyiv, 64/13, Volodymyrska Street, Kyiv 01601, Ukraine*
[2]*Vienna Center for Quantum Science and Technology, Atominstitut, TU Wien, Stadionallee 2, 1020 Vienna, Austria*
[3]*Technische Universität Darmstadt, Institut für Angewandte Physik, Schlossgartenstraße 7, 64289 Darmstadt, Germany*
[4]*Helmholtz Forschungsakademie Hessen für FAIR (HFHF), Campus Darmstadt, Schlossgartenstraße 2, 64289 Darmstadt, Germany*
[5]*Dipartimento di Fisica e Astronomia Galileo Galilei, Universitá di Padova, and INFN, Sezione di Padova, Via Marzolo 8, 35131 Padova, Italy*

(Received 17 November 2024; accepted 24 March 2025; published 14 April 2025)

Precise control of topologically protected excitations, such as quantum vortices in atomtronic circuits, opens new possibilities for future quantum technologies. We theoretically investigate the dynamics of Josephson vortices (rotational fluxons) induced by coupled persistent currents in a system of coplanar double-ring atomic Bose-Einstein condensates. We study the Josephson effect in an atomic Josephson junction formed by coaxial ring-shaped condensates. Tunneling superflows, initiated by an imbalance in atomic populations between the rings, are significantly influenced by the persistent currents in the inner and outer rings. This results in pronounced Josephson oscillations in the population imbalance for both corotating and nonrotating states. If a linear acceleration is applied to the system, our analysis reveals peculiar azimuthal tunneling patterns and dynamics of Josephson vortices which leads to nonzero net tunneling current and shows sensitivity to the acceleration magnitude. When multiple Josephson vortices are present, asymmetric vortex displacements that correlate with both the magnitude and direction of acceleration can be measured, offering the potential for quantum sensing applications.

DOI: 10.1103/PhysRevA.111.043308

I. INTRODUCTION

The Josephson effect, first predicted in superconductors [1,2], has been observed in a wide range of systems, with ring-shaped geometries attracting particular attention due to their ability to support persistent supercurrents. Over several decades, long Josephson junctions in superconducting rings and the dynamics of Josephson vortices (rotational fluxons) have been extensively studied, revealing fundamental aspects of phase-coherent transport and nonlinear excitations [3–15]. The realization of ac and dc Josephson effects in Bose-Einstein condensates (BECs) [16], along with subsequent advances in bosonic Josephson junctions [17], has expanded the study of quantum coherent phenomena beyond superconducting systems. In particular, atomic BECs confined in ring-shaped traps offer a highly controllable platform for the investigation of superfluid transport and topological excitations. As a consequence, persistent currents in toroidal atomic BECs have become a hallmark of macroscopic superfluidity, which have been extensively explored both theoretically and experimentally [18–30]. The toroidal geometry, with its central void, confines vortex cores and stabilizes even multicharged vortices. This robustness extends naturally to coupled superfluid rings, enabling the exploration of quantized angular momentum and Josephson vortices [31–48]. In these geometries, Josephson vortices emerge from phase differences across BEC junctions and manifest themselves as localized phase singularities within the tunneling region. The resulting robust, topologically protected excitations serve as building blocks for quantum sensing and atomtronic applications [49–52].

In this work, we investigate the dynamics of Josephson vortices in a dual coplanar ring configuration of atomic BECs (Fig. 1). We first examine the ac Josephson effect in coaxial toroidal condensates separated by a potential barrier, demonstrating that tunneling superflows, initiated by population imbalances, are strongly influenced by the persistent currents in both rings. When the rings share the same angular momentum state, pronounced Josephson oscillations emerge in the population imbalance, whereas differing angular momenta suppress the net current across the junction. We analyze the azimuthal pattern of the tunneling flow and the Josephson vortices within the circular junction. Finally, we show that linear acceleration induces asymmetric vortex displacement, providing a measurable signature for both the magnitude and direction of the acceleration.

The paper is organized as follows. Section II explores Josephson oscillations and vortex dynamics in a double-ring system. Section III examines vortex relaxation under acceleration, showing how stabilized Josephson vortices reveal its direction and magnitude. Section IV summarizes our findings.

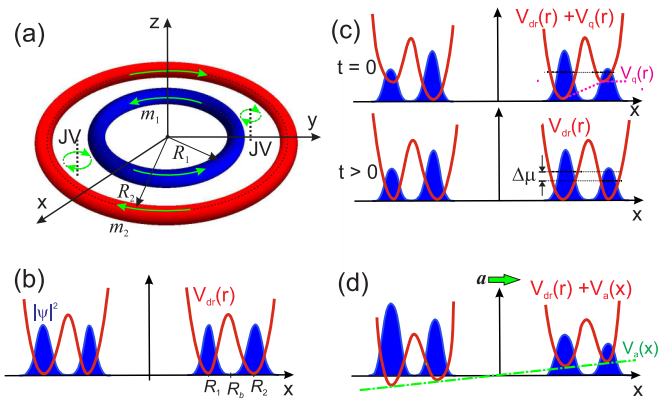

FIG. 1. (a) Schematic of the coplanar double-ring BEC with counterpropagating superflows (green arrows) and Josephson vortices (black dotted lines). (b) Potential profile $V_{dr}(r)$ (red) along the x axis, forming the double-ring trap and condensate density $|\psi|^2$ (blue). (c) Initial state at $t = 0$ showing the creation of chemical potential difference $\Delta\mu$ via initial bias potential $V_q(r)$ (magenta), quenched to the symmetric state for $t > 0$. (d) Uniform linear acceleration along the x axis (green arrow), with effective potential $V_a(x)$ (green dash-dotted line) inducing a density gradient.

II. JOSEPHSON OSCILLATIONS IN DOUBLE-RING SYSTEM

A. Model

The dynamical properties of a BEC within the mean-field theory at the zero-temperature limit is governed by the Gross-Pitaevskii equation (GPE)

$$i\hbar\frac{\partial\Psi(\mathbf{r},t)}{\partial t} = \left[-\frac{\hbar^2}{2M}\nabla^2 + V_{\text{ext}}(\mathbf{r}) + g|\Psi(\mathbf{r},t)|^2\right]\Psi(\mathbf{r},t), \tag{1}$$

where $g = 4\pi a_s\hbar^2/M$, $M = 1.44\times10^{-25}$ kg, and $a_s = 5.3\times10^{-9}$ m are the interaction strength, mass, and the s-wave scattering length of ^{87}Rb atoms. The wave function is normalized to the total number of atoms in the system

$$\int|\Psi(\mathbf{r},t)|^2 d\mathbf{r} = N. \tag{2}$$

The external trap potential V_{ext} forms the double-ring geometry of the system (see Fig. 1)

$$V_{\text{ext}}(\mathbf{r}) = \frac{1}{2}M\omega_z^2 z^2 + V_{dr}(r), \tag{3}$$

where $\omega_z = 2\pi\times 245$ Hz is the trapping frequency in a light sheet confining the atoms along the z direction. The radial trapping potential is given by

$$V_{dr}(r) = V_{\text{ring}}(r) + V_b(r), \tag{4}$$

where $r = \sqrt{x^2+y^2}$. The term $V_{\text{ring}}(r)$ defines a ring-shaped potential with a flattened bottom

$$V_{\text{ring}}(r) = V_1(r)\Theta(R_1 - r) + V_2(r)\Theta(r - R_2), \tag{5}$$

where the Heaviside step functions $\Theta(r)$ ensure that $V_{\text{ring}}(r) = 0$ for $R_1 < r < R_2$, while $V_{\text{ring}}(r) = V_1(r)$ for $0 \leqslant r \leqslant R_1$ and $V_{\text{ring}}(r) = V_2(r)$ for $r \geqslant R_2$. The potentials defining the inner and outer wells, $V_j(r)$ for $j = 1, 2$, take the form

$$V_j(r) = \frac{1}{2}M\omega_r^2(r - R_j)^2, \tag{6}$$

with identical trapping frequencies $\omega_r = 2\pi\times 110$ Hz and distinct ring radii $R_1 = 14$ μm, $R_2 = 24$ μm.

The term $V_b(r)$ represents the barrier separating the rings

$$V_b(r) = U_b\exp\left[-\frac{(r - R_b)^2}{2l_b^2}\right], \tag{7}$$

centered at $R_b = (R_1 + R_2)/2$. The barrier height U_b and width l_b are specified below.

The proposed radial double-ring potential (4) with a flattened bottom enables refined control of the interring barrier. Notably, such a trapping geometry can be readily implemented using existing experimental techniques, e.g., freely configurable dipole potentials generated by a digital micromirror device (DMD).

We analyze tunneling flows based on the direct numerical simulations of the two-dimensional (2D) GPE for a setup of coplanar rings, assuming tight confinement along the z-axis, so that bending and tilting of vortices are suppressed, allowing for a 2D approximation

$$\Psi(\mathbf{r},t) = e^{-i\mu t/\hbar}\psi(x,y,t)\zeta(z,t), \tag{8}$$

with

$$\zeta(z,t) = \left(\frac{1}{\sqrt{\pi}l_z}\right)^{1/2}\exp\left(-\frac{z^2}{2l_z^2} - i\frac{\omega_z t}{2}\right), \tag{9}$$

where $l_j = \sqrt{\hbar/(M\omega_j)}$, $j = z, r$, and where μ is the total chemical potential of the 2D stationary state of the double-ring system. Integrating (1) with this ansatz over z and applying the following transformations $t \to \omega_r t$, $(x, y) \to (x, y)/l_r$, $V \to V/(\hbar\omega_r)$, $\mu \to \mu/(\hbar\omega_r)$, $\psi \to l_r\psi$, the dimensionless 2D GPE can be written as

$$i\frac{\partial\psi}{\partial t} = \left(-\frac{1}{2}\nabla^2 + V_{\text{ext}} + g_{2D}|\psi|^2 - \mu\right)\psi, \tag{10}$$

where $g_{2D} = \sqrt{8\pi}a_s/l_z$ is the dimensionless coupling and μ is the chemical potential of the steady state $\tilde{\psi}$, which satisfies the stationary GPE: $\hat{\mathcal{H}}\tilde{\psi} = \mu\tilde{\psi}$ with

$$\hat{\mathcal{H}} = -\tfrac{1}{2}\nabla^2 + V_{\text{ext}} + g_{2D}|\tilde{\psi}|^2. \tag{11}$$

The wave function $\tilde{\psi}(x, y)$ of the stationary state of the condensate in the double-ring potential $V_{dr}(r)$ is obtained by the imaginary time propagation method. The total number of atoms $N = N_1^{(0)} + N_2^{(0)}$ is distributed between inner and outer rings

$$N_j^{(0)} = \iint_{S_j}|\tilde{\psi}|^2 dxdy, \tag{12}$$

with integration boundaries for the inner ring, S_1: $0 \leqslant r < R_b$ and for the outer ring, S_2: $r \geqslant R_b$. The radial double-well potential $V_{dr}(r)$ traps an azimuthally symmetric double-ring condensate and splits it into two parts.

We define the population imbalance between these parts as the deviation in the number of particles from their equilibrium

values, $N_j^{(0)}$, as

$$\Delta N(t) = \left[N_2(t) - N_2^{(0)}\right] - \left[N_1(t) - N_1^{(0)}\right], \tag{13}$$

and introduce the chemical potentials of each ring as

$$\mu_j = \frac{1}{N_j} \iint_{S_j} \psi^* \hat{\mathcal{H}} \psi, \tag{14}$$

where $\hat{\mathcal{H}}$ is the system's Hamiltonian (11).

B. Initial bias potential

The initial population imbalance and chemical potential difference $\Delta\mu = \mu_1 - \mu_2$ between the rings is generated by applying an additional initial bias potential, following methods similar to those used in double-well experiments [16]. The total external potential consists of both the trapping potential and the initial bias potential, as illustrated in Fig. 1(c). The latter is given by

$$V_q(r) = \begin{cases} b_1, & 0 \leqslant r < R_1, \\ (b_2 - b_1)\frac{r-R_1}{R_2-R_1} + b_1, & R_1 \leqslant r < R_2, \\ b_2, & R_2 \leqslant r, \end{cases} \tag{15}$$

where $b_{1,2}$ are the potential offsets applied to the two rings to induce a chemical potential difference $\Delta\mu$.

In our simulations, the initial state is prepared as a stationary solution with $b_1 = 0$ and $b_2 \neq 0$, effectively shifting the outer ring and controlling $\Delta\mu$ via b_2. To initiate the dynamics, we rapidly switch off the initial bias potential and observe the subsequent evolution of the condensate in the double-ring system using the conservative GPE (10).

C. Josephson oscillations at zero acceleration

First, we investigate the ac Josephson effect in a double-ring system, characterized by a constant chemical potential difference that drives oscillatory tunneling of atoms between the rings. A distinctive feature of it is that the frequency of the population imbalance is directly proportional to the applied chemical potential difference, while the phase difference increases linearly over time: $\Phi(t) = \Phi_0 + \omega_{\Delta N} t$. In our simulations the population imbalance oscillates with a frequency $\omega_{\Delta N} = \Delta\mu/\hbar$ for high-enough initial chemical potential difference (see Fig. 3). These properties of the ac Josephson effect are observed in both nonrotating states and states with persistent currents, provided the rings have the same angular momentum state ($m_1 = m_2$).

We conducted an extensive series of numerical simulations of Josephson oscillations, varying the number of particles in the rings and the initial chemical potential difference. Figure 2 showcases the pronounced oscillations and the radial flow structure for $N = 5 \times 10^5$. Figure 2(b) specifically illustrates the $\Delta N(t)$ oscillations observed in the time-dependent GPE simulations for nonrotating rings ($m_1 = m_2 = 0$).

Remarkably, persistent currents with $m_1 \neq m_2$ result in a nearly constant $\Delta N(t)$ with no visible oscillations, as depicted in Fig. 2(b).

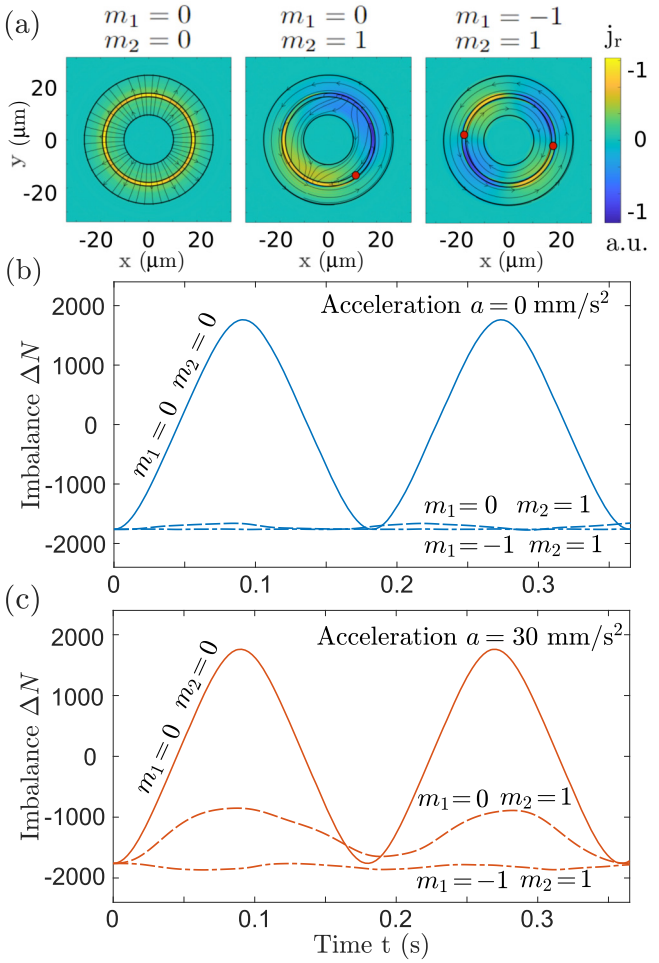

FIG. 2. (a) Flow density snapshots for different angular momentum states: $m_1 = m_2 = 0$ shows purely radial tunneling; $m_1 = 0$, $m_2 = 1$ forms one vortex, highlighted by a red circle; $m_1 = -1$, $m_2 = 1$ results in two vortices. (b) Particle number imbalance for $m_1 = 0$, $m_2 = 0$ (solid blue, pronounced tunneling), $m_1 = 0$, $m_2 = 1$ and $m_1 = -1$, $m_2 = 1$ (dashed and dash-dotted blue, suppressed tunneling). (c) Linear acceleration induces imbalance oscillations for $m_1 = 0$, $m_2 = 1$ (dashed red) but not for counter-propagating flows (dash-dotted red). Tunneling for $m_1 = 0$, $m_2 = 0$ is preserved (solid red). $U_b = 49\,\hbar\omega_r = 4.25\,\mu_0$, $l_b = 0.33\,\mu$m, $N = 5 \times 10^5$.

Numerical solutions of the GPE were used to calculate the superfluid-flow density as

$$\mathbf{j} = \frac{i\hbar}{2M}[\Psi\nabla\Psi^* - \Psi^*\nabla\Psi]. \tag{16}$$

Figure 2(a) illustrates the radial flow distribution j_r in the (x, y) plane for different angular momentum states. The suppression of the total tunneling flow is accompanied by the emergence of $N_{\mathrm{JV}} = |m_1 - m_2|$ Josephson vortices, marked by red circles in Fig. 2(a). This effect arises from the azimuthal symmetry of the tunneling flow, as previously analyzed in Refs. [42,44,53] for vertically stacked ring condensates. Figure 2(a) shows the color-coded radial flow component j_r in the planar double-ring system. Note that for $m_1 = 0$ and $m_2 = 1$, a single Josephson vortex resides in the

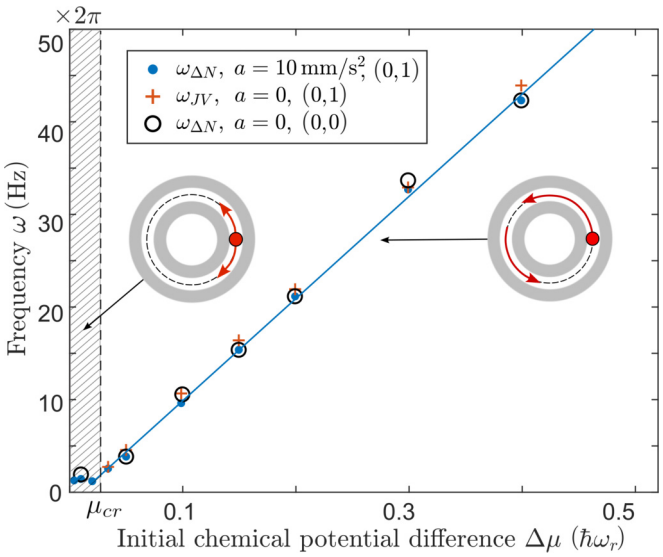

FIG. 3. Oscillation frequency ω of the population imbalance versus chemical potential difference $\Delta\mu$ for $(m_1 = 0,\ m_2 = 1)$ with $a = 10\,\mathrm{mm/s^2}$ (blue dots) and $(m_1 = m_2 = 0)$ without acceleration (black circles), fitted linearly. Vortex rotation frequencies for $m_1 = 0$, $m_2 = 1$ state are marked by red crosses. $U_b = 7\,\hbar\omega_r$, $l_b = 1\,\mu\mathrm{m}$, $N = 5 \times 10^4$.

barrier, even though two diametrically opposed points exhibit zero radial flow. The vortex is identified by its circulating condensate flow, forming a closed loop around its core, whereas the other zero-flow point does not support such circulation.

D. Josephson oscillations under linear acceleration

Next, let us consider the effect of acceleration which breaks the azimuthal symmetry and causes a redistribution of density and radial flows. Acceleration introduces an inertial force that affects the condensate, similar to how a classical fluid or gas in a container shifts when the container is accelerated. This force is defined by the gradient of an effective potential that pulls atoms in the opposite direction of acceleration. As shown in Fig. 1(d), this leads to a density gradient, with atoms accumulating slightly more on one side. As we demonstrate in this section, such density redistribution influences the tunneling between the rings and affects the motion of Josephson vortices.

To analyze the effects of external acceleration, we transform to an accelerating reference frame comoving with the system. Following the approach in Ref. [54], where a similar transformation was applied to a dissipative system, we introduce the change of variables $\mathbf{r}' = \mathbf{r} - \mathbf{r}_0(t)$ in (1), where $\mathbf{r}_0(t)$ represents the origin of the new frame moving with constant linear acceleration $\mathbf{a} = d^2\mathbf{r_0}/dt^2$. Applying the gauge transformation

$$\Psi'(\mathbf{r}', t) = e^{i\Phi/\hbar}\Psi(\mathbf{r}', t), \tag{17}$$

with

$$\Phi = \mathbf{p}_0(t)\cdot\mathbf{r}' + \frac{1}{2M}\int_0^t \mathbf{p}_0^2(\tau)d\tau, \tag{18}$$

where $\mathbf{p}_0(t) = Md\mathbf{r}_0(t)/dt$, we obtain the additional effective potential in GPE (1) as

$$V_a = M(\mathbf{a}\cdot\mathbf{r}'), \tag{19}$$

which accounts for the inertial force. For clarity, we omit the primes in Ψ' and $\mathbf{r}'$ hereafter.

In our simulations, acceleration is incorporated by adding the effective potential $V_a = Max/(\hbar\omega_r)$ to dimensionless 2D GPE (10), corresponding to a uniform horizontal acceleration $\mathbf{a} = (a, 0)$. This potential naturally emerges from the transformation to an accelerating reference frame, ensuring a consistent description of the dynamics in a noninertial reference frame.

We prepare the initial state with the applied effective potential (19) and introduce the chemical potential difference using the initial bias potential procedure described above. The results of the numerical simulations for nonzero acceleration are shown in Figs. 2(c) and 3. The frequency of the oscillations for nonrotating rings is shifted by acceleration, consistent with the recent study of a one-dimensional (1D) system of N bosons in an accelerated double-well potential [55]. However, the most pronounced effect of acceleration is observed in the tunneling dynamics between rings with different angular momenta. As discussed below, these effects can be explained by the azimuthal symmetry breaking induced by constant linear acceleration.

E. Two-mode model

To gain deeper insight into the tunneling flow mechanism between the condensate rings, we adopt a simplified two-mode approximation model. In this approach, we substitute the following ansatz for the 2D wave function into (16):

$$\Psi = \psi_1(r)e^{i\mu_1 t + im_1\varphi} + \psi_2(r)e^{i\mu_2 t + im_2\varphi}, \tag{20}$$

where $\psi_{1,2}$ are the wave functions of the condensate in the rings, $\mu_{1,2}$ are their chemical potentials, and $m_{1,2}$ represent the vorticities of the rings. Through straightforward algebra, we obtain very simple relation for the radial flow density

$$j_r(r, \varphi, t) = j_0 \sin(\Delta\mu t - \Delta m\varphi), \tag{21}$$

where $\Delta m = m_1 - m_2$, and $j_0 = j_0(r)$ is a function of the radial coordinate only, assuming an azimuthally symmetric density distribution $(a = 0)$. The effect of acceleration-induced density variations can be taken into account by modifying the amplitude factor as $j_0(r)(1 - \delta_a\cos\varphi)$, where $\delta_a \ll 1$ is a dimensionless parameter that accounts for the small density bias introduced by linear acceleration.

It is evident that the total flow through the junction $J(t) = \int j_r\, d^2\mathbf{r}$ vanishes if the number of vortices is not zero or one. Specifically, $J(t) = J_0\sin(\Delta\mu t)$ for $\Delta m = 0$, corresponding to ac Josephson oscillations, which are present for both zero and nonzero accelerations, with the frequency defined by the chemical potential difference. Remarkably, for $\Delta m = \pm 1$ and under external acceleration, the total tunneling flow is also nonzero: $J = \frac{1}{2}\delta_a J_0\sin(\Delta\mu t)$, although the amplitude of the flow is reduced to the small factor δ_a. Therefore, we can conclude, that for $\Delta m = 0$ (no vortices), population imbalance oscillations occur for both zero and nonzero acceleration a. For $\Delta m = \pm 1$ (one vortex), these oscillations are suppressed

at $a = 0$ but persist for $a \neq 0$. For $\Delta m \geqslant 2$ (two or more vortices), the oscillations remain suppressed in both cases.

The numerical simulations presented in Figs. 2(b) and 2(c) confirm these predictions. Specifically, in the $m_1 = 0, m_2 = 1$ state, population imbalance oscillations, which are suppressed at zero acceleration [dashed blue in Fig. 2(b)], reappear for $a \neq 0$ due to $\Delta m = 1$ [dashed red in Fig. 2(c)]. In contrast, in the $m_1 = -1, m_2 = 1$ state, oscillations remain suppressed [dash-dotted lines in Figs. 2(b) and 2(c)], in full agreement with the theoretical predictions.

The dependence of the Josephson effect oscillation frequency $\omega_{\Delta N}$ on the initial chemical potential difference $\Delta\mu$ is depicted in Fig. 3. Here and further, we use a barrier width of $l_b = 1\,\mu$m and the total particle number of $N = 5 \times 10^4$. Figure 3 shows the frequency of population imbalance oscillations, $\omega_{\Delta N}$ for two cases: (i) open circles depict $a = 0$, $\Delta m = 0$, and (ii) blue dots correspond to $a = 10\,\mathrm{mm/s^2}$, $\Delta m = 1$. The red crosses indicate the angular frequency ω_{JV} of the vortex circulation in the barrier. Note that all three data sets fit the same linear behavior $\omega_{\Delta N} \sim \Delta\mu$ inherent to the ac Josephson effect for $\Delta\mu > \mu_{\mathrm{cr}}$.

Figure 3 also reveals the two relevant regimes of vortex motion depending on the additional energy provided by the initial chemical potential difference $\Delta\mu$, separating at $\Delta\mu = \mu_{\mathrm{cr}}$. The frequency of Josephson oscillations is a linear function of the chemical potential difference if the initial imbalance is above a certain critical value μ_{cr}. This regime corresponds to the circular motion of the vortex within the barrier. The frequency ω_{JV} of its circular motion in the barrier matches the frequency of the population imbalance $\omega_{\Delta N}$. Below the critical value μ_{cr} of the chemical potential difference, the frequency remains constant, corresponding to periodic oscillations of the Josephson vortex around the equilibrium position.

F. Energetic analysis

We used the energetic analysis for the vortex position along the annulus (Fig. 4) and found two distinct regimes of its dynamics: (i) circular motion in the barrier and (ii) oscillations in the vicinity of the position with minimum energy. Let us show the connection between these characteristics and an external linear acceleration. To this end, we use the dependence of the BEC energy on the azimuthal position of the vortex in the ring.

Within the approximation of the constant local density of the unperturbed condensate (state $m_1 = m_2 = 0$, ψ_0) in the vicinity of the vortex position, we can write the wave function of the state with imprinted vortex ($m_1 = 0$, $m_2 = 1$, ψ_{v}) through the wave function of the vortex in the homogeneous condensate and the unperturbed state ψ_0 as

$$\psi_{\mathrm{v}}(\mathbf{r}) = A\psi_0(\mathbf{r}) \tanh\left(\frac{\varrho}{\xi}\right) e^{i\theta}, \tag{22}$$

where $\varrho = |\mathbf{r} - \mathbf{r}_{\mathrm{JV}}|$ is the distance from the vortex core located in $\mathbf{r}_{\mathrm{JV}}$, $\theta = \arg(\mathbf{r} - \mathbf{r}_{\mathrm{JV}})$ is the angle relative to the core, A is the normalization constant, and ξ is the healing length. Since the vortex is localized radially at the center of the barrier $r_{\mathrm{JV}} = R_b$, thus its position and energy are uniquely determined by the angular position φ_{JV}.

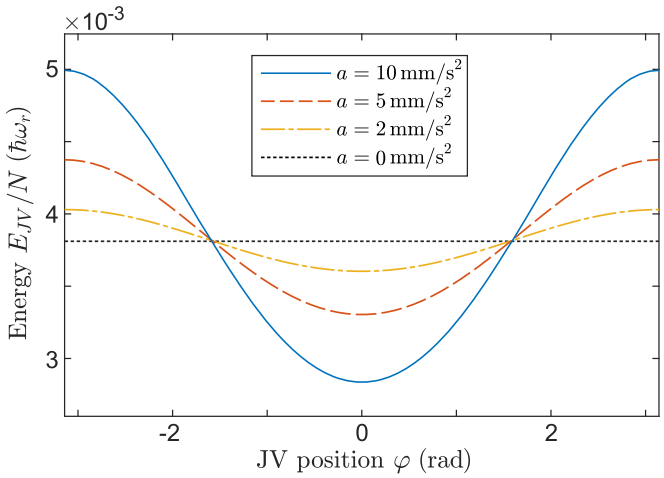

FIG. 4. Nucleation energy per particle E_{JV}/N for the single vortex between rings as a function of its angular position φ. The acceleration-induced density gradient generates a nucleation energy minimum for the vortex, in the direction of the acceleration, i.e., $\varphi_a = 0$. $U_b/\mu = 1.5$, $l_b = 1.43\,\mu$m, $N = 5 \times 10^4$.

The total energy of the BEC in the state ψ is given as follows:

$$E(\psi) = \int \left(\frac{1}{2}|\nabla\psi|^2 + V_{\mathrm{ext}}|\psi|^2 + \frac{g}{2}|\psi|^4\right) d^2\mathbf{r}. \tag{23}$$

The external potential V_{ext} consists of both the trapping potential and the effective potential associated with the applied acceleration (19).

Let us introduce a nucleation energy of the vortex, defined as the difference of the energy of the state with imprinted Josephson vortex line ψ_{v} and the ground-state energy

$$E_{\mathrm{JV}} = E(\psi_{\mathrm{v}}) - E(\psi_0). \tag{24}$$

Figure 4 illustrates the nucleation energy per particle E_{JV}/N as the function of the angular coordinate of the vortex core. In this scenario, the characteristics of the vortex energy are strongly influenced by the applied acceleration. The energy minimum occurs in the direction of the applied acceleration, with its depth being proportional to the magnitude of the acceleration $|\mathbf{a}|$.

The characteristics of the acceleration-induced E_{JV} minimum are reflected in the dynamics of the BEC, particularly in the azimuthal motion of the vortex along the barrier between rings, $\varphi_{\mathrm{JV}}(t)$, as illustrated in Fig. 5. The vortex and antivortex circulate in opposite directions at zero acceleration. However, as shown in the next section and illustrated in Fig. 5(b), for the system with dissipation, the angular positions of both the vortex (solid red line) and the antivortex (dashed red line) ultimately align with the direction of the applied acceleration. By examining the features of this motion, one can extract both the direction and magnitude of the applied acceleration, thus offering a mechanism for acceleration sensing based on the Josephson vortex dynamics.

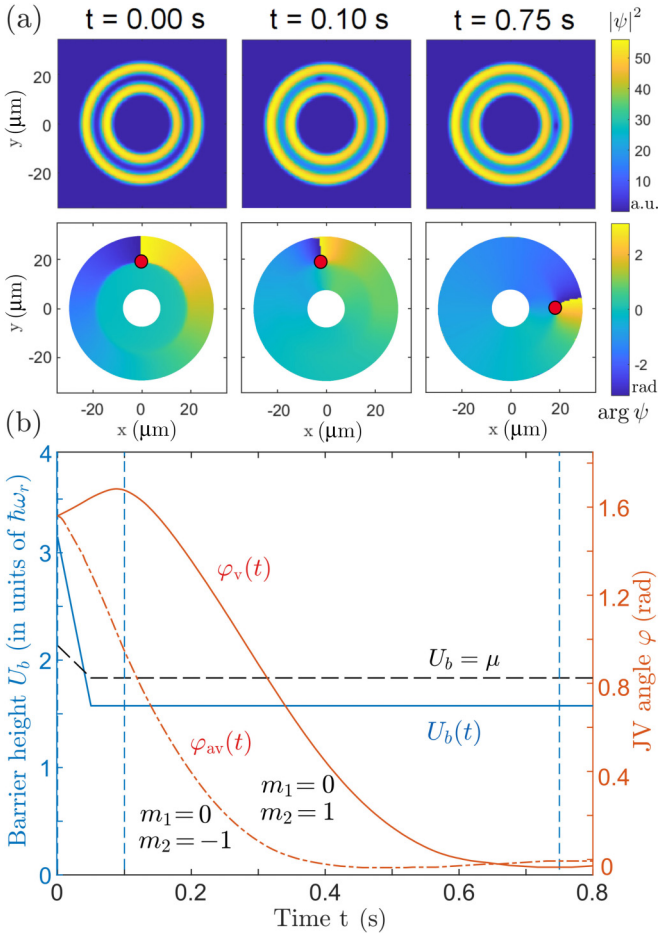

FIG. 5. (a) Dynamics of a single vortex (red circle indicates position of its core) under constant horizontal acceleration $a = 2\,\mathrm{mm/s^2}$ ($\varphi_a = 0$), $l_b = 1.43\,\mu\mathrm{m}$, and $N = 5 \times 10^4$, showing density (upper row) and phase (lower row) evolution. The vortex aligns with the acceleration, stabilizing at $\varphi = \varphi_a = 0$ due to nonzero dissipation $\gamma = 0.015$. (b) Barrier amplitude $U_b(t)$ and vortex angular coordinate $\varphi(t)$ versus time. Starting at $t = 0$, the barrier amplitude U_b is ramped down over 0.05 s from $1.5\,\mu_0$ to $0.75\,\mu_0$, where $\mu_0 = \mu(0)$, and then remains unchanged (blue solid line). The red lines show the angular coordinate over time for vortex (red solid line) and antivortex (red dash-dotted line). The black dashed line denotes the barrier amplitude at the chemical potential level $U_b = \mu(t)$.

III. DISSIPATIVE DYNAMICS OF JOSEPHSON VORTICES

Dissipative effects are crucial in modeling nonequilibrium behavior, such as vortex nucleation, as they drive relaxation to equilibrium. Dissipation causes the vortex line to drift to the condensate edge (where vortices decay) or to pin it in the central hole of a ring-shaped condensate. Relaxation of the vortex core to the local energy minimum forms a metastable persistent current. In a trapped condensate, these effects arise from interaction with a thermal cloud and are phenomenologically described by the dissipative Gross-Pitaevskii equation (DGPE) [56,57]. For weakly interacting degenerate atoms near the thermodynamic equilibrium and under weak dissipation, the DGPE for the macroscopic wave function is given by

$$(i - \gamma)\frac{\partial \Psi}{\partial t} = [\hat{\mathcal{H}} - \mu]\Psi, \tag{25}$$

where $\gamma \ll 1$ is the dissipation rate. The dissipation rate γ determines the relaxation time of the system to a (meta)stable state: the larger γ, the shorter the relaxation time, but the final state does not depend on the specific value of γ. Thus, our main results are qualitatively independent of the chosen value of γ. Furthermore, we analyze a wide range of its values covering different types of dynamics from conservative case ($\gamma = 0$) to rather strong dissipation related to estimates obtained in Ref. [56]. Notably, the introduction of phenomenological dissipation in this manner accounts for dissipation within an accelerating frame, where the thermal cloud is assumed to comove with the condensate. A detailed discussion of physically relevant approaches to incorporating dissipation under acceleration is provided in Ref. [54]. Importantly, the phenomenological dissipation rate γ remains independent of acceleration in a noninertial accelerated frame. While an additional effective potential arises in this setting, the dissipation parameter γ remains unchanged by acceleration or rotation, as demonstrated in Ref. [58]. In our dynamical simulations, the chemical potential $\mu(t)$ of the equilibrium state is adjusted at each time step to conserve the number of particles N.

One of the key features of quantum vortices, as topologically protected states, is their inherent stability. Both theoretical [43,59] and experimental [47,48] studies demonstrated that a merging double-ring system exhibits the formation of spiral interference patterns associated with vortex flows. These patterns provide a robust and accessible method for measuring the angular momentum state of toroidal condensates.

Very recently, a side-by-side configuration of two rings connected by a tunable weak link was proposed as a physical platform for creating acceleration [54] and rotation [60] sensors, based on a threshold-driven vortex transfer approach previously introduced in Ref. [61]. In this setup, the barrier amplitude directly modulates vortex transitions, enabling discrete, measurable shifts that can be finely controlled, or even halted, by tuning the barrier strength.

In this work, we investigate the behavior of a double-ring system subjected to constant linear acceleration, which breaks the symmetry of the system and consequently leads to an asymmetric arrangements of the tunneling currents. It is therefore expected that locations of vortex cores inside the circular barrier can be explicitly related to the direction and magnitude of the acceleration. In our simulations we use unbiased ($\Delta\mu = 0$) double-ring system with barrier amplitude $U_b > \mu$ as the initial condition. To detect the vortex positions in both the density and phase distributions, we reduce the barrier amplitude to a constant value just below the chemical potential, as shown in Fig. 5, with a time constant long enough to suppress the formation of spiral structures. As a result of the relaxation process, we observe stationary vortex positions that exhibit sensitivity to the applied acceleration.

Linear acceleration induces an azimuthal asymmetry in the density distribution, making the angular position aligned with the acceleration direction energetically favorable for the vortex, as illustrated in Fig. 4. Notably, the local energy minima

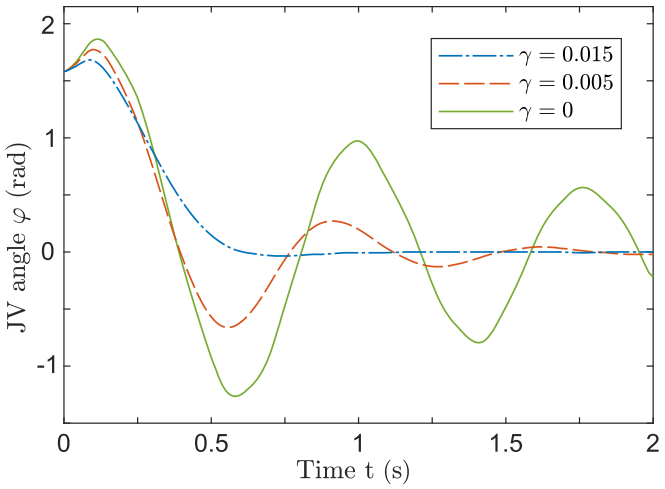

FIG. 6. Angular dynamics of a single vortex under constant acceleration $a = 2\,\mathrm{mm/s^2}$ for different dissipation rates γ, with $\varphi_a = 0$. Higher γ reduces the relaxation time of the vortex at $\varphi = \varphi_a$, aligned with the acceleration for $l_b = 1.43\,\mu\mathrm{m}$, $N = 5 \times 10^4$.

deepen with increasing acceleration. Consequently, in a conservative system, the Josephson vortex either circulates within the lower-density region between the rings at low acceleration rates or undergoes periodic oscillations along the direction of acceleration when the acceleration is sufficiently high for a given chemical potential difference.

In realistic experiments at finite temperature, interactions between the condensate and the thermal cloud introduce dissipative effects, which cause the vortex angular position to eventually align with the direction of acceleration after a relaxation period. An additional mechanism contributing to the decay of its oscillations, even for $\gamma = 0$, is the emission of acoustic waves during vortex drift in an inhomogeneous condensate [62]. Figure 6 illustrates the evolution of the vortex angular position in both conservative and dissipative regimes. As expected, increasing the dissipation rate γ accelerates the relaxation process.

The motion of Josephson vortices in an accelerating frame is governed by the interplay between their effective mass and the energy landscape, as previously analyzed in the context of superfluid junctions and fluxon dynamics [38,63]. In our system, acceleration shifts the nucleation energy minimum, leading to the preferential alignment of vortices in the direction of the applied acceleration (see Figs. 4–7).

We quantify the asymmetry of the vortex lattice by the relative deviation of its centroid $d = |\mathbf{d}|$, which describes the collective displacement of all vortices

$$\mathbf{d} = \frac{1}{N_{\mathrm{JV}}} \sum_{n=1}^{N_{\mathrm{JV}}} \frac{\mathbf{r}_n}{R_b}, \tag{26}$$

where $\mathbf{r}_n$ is the radius vector of the nth vortex, N_{JV} is the total number of vortices, and R_b is the radius of the circular barrier, where they are located.

In the absence of acceleration, all vortices are symmetrically positioned at the vertices of a regular n-gon, resulting in zero relative deviation ($|\mathbf{d}| = d = 0$). When acceleration is applied, they shift in the direction of the acceleration,

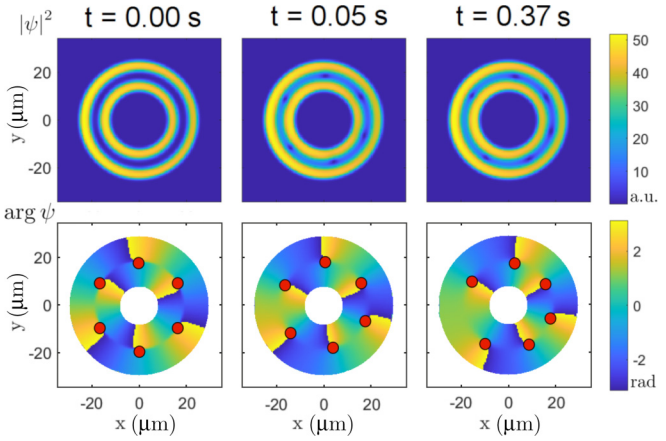

FIG. 7. Density (upper row) and phase (lower row) snapshots of two coaxial rings with six vortices under a constant horizontal acceleration of $a = 2\,\mathrm{mm/s^2}$ and dissipation rate $\gamma = 0.015$ at various times after lowering the barrier height. Their cores are marked by red circles. Initially symmetric, the vortex lattice is deformed by acceleration, stabilizing into an asymmetrical configuration. During the first $t = 0.05\,\mathrm{s}$, the interring barrier is linearly lowered to facilitate imaging of vortices and pinning them in the radial direction.

$\mathbf{d} \parallel \mathbf{a}$, $d > 0$, finding a new equilibrium position influenced by mutual repulsion (as all vortices have the same sign). After equilibration, the system exhibits an intermediate asymmetry $0 \leqslant d < 1$, pointing towards the direction of acceleration. A typical example of the evolution of a lattice formed by six vortices is shown in Fig. 7.

The equilibration of the system with a nonzero dissipation rate γ enables us to determine the actual value of the asymmetry parameter d in the equilibrium state of the vortex chain. It is essential to ensure that the equilibrium value of d is independent of the specific dissipation rate used. To verify

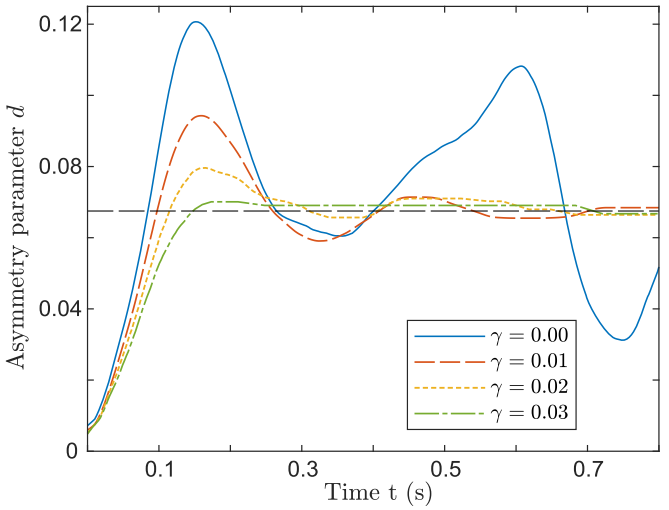

FIG. 8. Evolution of the asymmetry parameter d for six vortices under constant acceleration $a = 2\,\mathrm{mm/s^2}$, $l_b = 1.43\,\mu\mathrm{m}$, $N = 5 \times 10^4$ for various dissipation rates γ. While γ affects the equilibration dynamics of d (exhibiting decaying oscillations for $\gamma \leqslant 0.025$ and becoming aperiodic for $\gamma > 0.025$) the equilibrium asymmetry value remains independent of the dissipation rate.

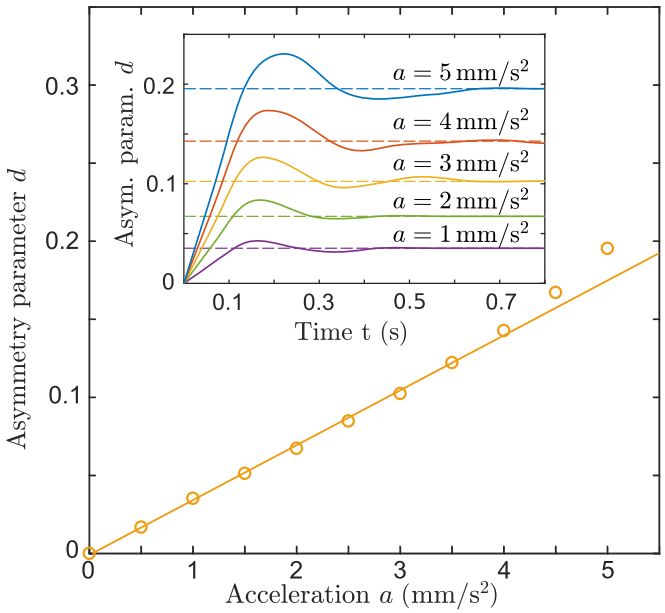

FIG. 9. Equilibrium asymmetry parameter d as a function of linear acceleration a, illustrating a linear dependence at low accelerations for $l_b = 1.43\,\mu$m, $N = 5 \times 10^4$. (Inset) Time evolution of the asymmetry parameters for varying accelerations a (solid lines) with their respective equilibrium values for $\gamma = 0.015$ (dashed lines).

this, we compared the evolution of six vortices with different dissipation rates from $\gamma = 0$ to $\gamma = 3 \times 10^{-2}$ and confirmed that the final equilibrium value of d does not depend on γ (see Fig. 8). For our simulations, we use an intermediate value of $\gamma = 1.5 \times 10^{-2}$ for dissipation.

The equilibrium asymmetry parameter d shows a linear dependence on the applied acceleration a, following the relation $d = 3.52 \times 10^{-2}\,\mathrm{s^2/mm} \times a$ (see Fig. 9) for small accelerations. However, for $a \gtrsim 4.5\,\mathrm{mm/s^2}$, a deviation from this linear behavior is observed, likely due to the significant asymmetric density bias in the barrier region. As typically intended of quantum sensing devices, low acceleration rates are accessible to measurements, with the sensitivity of this method being limited at very low accelerations as the variation in the asymmetry parameter approaches the detection resolution limits of the vortex core positions. Conversely, measuring higher acceleration rates necessitates longer relaxation times, which prolongs the measurement process. Additionally, at very high acceleration rates, density biases may cause the ring-shaped condensate to break apart, further restricting the maximum accessible acceleration rate.

IV. CONCLUSION

In the present work we considered the ac Josephson effect in coaxial two-dimensional ring-shaped condensates separated by a potential barrier and investigated the dynamics of Josephson vortices within such a double-ring BEC. Through direct simulations of the Gross-Pitaevskii equation, we analyzed tunneling superflows driven by an initial imbalance in atomic populations of the rings. The superflows through the Bose-Josephson junction were strongly influenced by persistent currents in the concentric rings, leading to pronounced Josephson oscillations in population imbalances for corotating and nonrotating states. The azimuthal configuration of the tunneling flow required the formation of Josephson vortices, resulting in zero net current through the junction for rings with different angular momentum states. However, if a linear acceleration was applied to the system and there was only one vortex in the junction, the population imbalance oscillations can be restored.

A key aspect of this study was exploring how linear acceleration affects the dynamics of Josephson vortices. We found that acceleration leads to an asymmetric displacement of vortices, an effect that can be utilized to determine both the magnitude and direction of the acceleration. By introducing an asymmetry parameter for the vortex lattice after equilibration, we demonstrated that this parameter was linearly proportional to the absolute value of the applied acceleration. We prove that the equilibrium angular position of a single vortex was sensitive to the direction of acceleration.

These findings provide additional insights into the Josephson effect in a bosonic junction modified by linear acceleration and introduce prospective methods for quantifying acceleration effects via analysis of interference patterns experimentally observed in atomtronic systems [47,64,65].

ACKNOWLEDGMENTS

The authors thank Luca Salasnich, Yelyzaveta Nikolaieva, Mark Edwards, Andriy Chaika, and Yuriy Bidasyuk for useful discussions. Y.B., O.P., N.B., and A.Y. acknowledge support from the National Research Foundation of Ukraine through Grant No. 2020.02/0032. A.Y. acknowledges support from the project "Theoretical analysis of quantum atomic mixtures" of the University of Padova and from INFN.

[1] B. D. Josephson, Possible new effects in superconductive tunnelling, Phys. Lett. **1**, 251 (1962).
[2] A. Barone and G. Paterno, Physics and applications of the Josephson effect, J. Vac. Sci. Technol. **21**, 1050 (1982).
[3] D. Tilley, Cylindrical Josephson junctions, Phys. Lett. **20**, 117 (1966).
[4] P. Burt and M. Sherrill, The dc Josephson current in cylindrical junctions, Phys. Lett. A **85**, 97 (1981).
[5] M. D. Sherrill and M. Bhushan, Cylindrical Josephson tunneling, Phys. Rev. B **19**, 1463 (1979).
[6] A. Davidson, B. Dueholm, and N. F. Pedersen, Experiments on soliton motion in annular Josephson junctions, J. Appl. Phys. **60**, 1447 (1986).
[7] A. V. Ustinov, T. Doderer, R. P. Huebener, N. F. Pedersen, B. Mayer, and V. A. Oboznov, Dynamics of sine-gordon solitons in the annular Josephson junction, Phys. Rev. Lett. **69**, 1815 (1992).
[8] Z. Hermon, A. Stern, and E. Ben-Jacob, Quantum dynamics of a fluxon in a long circular Josephson junction, Phys. Rev. B **49**, 9757 (1994).

[9] A. V. Ustinov, Observation of a radiation-induced soliton resonance in a Josephson ring, JETP Lett. **64**, 191 (1996).

[10] A. V. Ustinov, B. A. Malomed, and E. Goldobin, Backbending current-voltage characteristic for an annular Josephson junction in a magnetic field, Phys. Rev. B **60**, 1365 (1999).

[11] S. Watanabe, H. S. van der Zant, S. H. Strogatz, and T. P. Orlando, Dynamics of circular arrays of Josephson junctions and the discrete sine-gordon equation, Physica D **97**, 429 (1996).

[12] E. Trías, J. J. Mazo, F. Falo, and T. P. Orlando, Depinning of kinks in a Josephson-junction ratchet array, Phys. Rev. E **61**, 2257 (2000).

[13] A. V. Ustinov, Fluxon insertion into annular Josephson junctions, Appl. Phys. Lett. **80**, 3153 (2002).

[14] A. V. Ustinov, C. Coqui, A. Kemp, Y. Zolotaryuk, and M. Salerno, Ratchet-like dynamics of fluxons in annular Josephson junctions driven by biharmonic microwave fields, Phys. Rev. Lett. **93**, 087001 (2004).

[15] M. V. Fistul, A. Wallraff, Y. Koval, A. Lukashenko, B. A. Malomed, and A. V. Ustinov, Quantum dissociation of a vortex-antivortex pair in a long Josephson junction, Phys. Rev. Lett. **91**, 257004 (2003).

[16] S. Levy, E. Lahoud, I. Shomroni, and J. Steinhauer, The ac and dc Josephson effects in a Bose-Einstein condensate, Nature (London) **449**, 579 (2007).

[17] M. Pigneur, T. Berrada, M. Bonneau, T. Schumm, E. Demler, and J. Schmiedmayer, Relaxation to a phase-locked equilibrium state in a one-dimensional Bosonic Josephson junction, Phys. Rev. Lett. **120**, 173601 (2018).

[18] C. Ryu, M. F. Andersen, P. Cladé, V. Natarajan, K. Helmerson, and W. D. Phillips, Observation of persistent flow of a Bose-Einstein condensate in a toroidal trap, Phys. Rev. Lett. **99**, 260401 (2007).

[19] C. Ryu, P. W. Blackburn, A. A. Blinova, and M. G. Boshier, Experimental realization of Josephson junctions for an atom squid, Phys. Rev. Lett. **111**, 205301 (2013).

[20] C. Ryu, E. C. Samson, and M. G. Boshier, Quantum interference of currents in an atomtronic SQUID, Nat. Commun. **11**, 3338 (2020).

[21] S. Moulder, S. Beattie, R. P. Smith, N. Tammuz, and Z. Hadzibabic, Quantized supercurrent decay in an annular Bose-Einstein condensate, Phys. Rev. A **86**, 013629 (2012).

[22] F. Piazza, L. A. Collins, and A. Smerzi, Vortex-induced phase-slip dissipation in a toroidal Bose-Einstein condensate flowing through a barrier, Phys. Rev. A **80**, 021601(R) (2009).

[23] F. Piazza, L. A. Collins, and A. Smerzi, Current-phase relation of a Bose-Einstein condensate flowing through a weak link, Phys. Rev. A **81**, 033613 (2010).

[24] A. Ramanathan, K. C. Wright, S. R. Muniz, M. Zelan, W. T. Hill, C. J. Lobb, K. Helmerson, W. D. Phillips, and G. K. Campbell, Superflow in a toroidal Bose-Einstein condensate: An atom circuit with a tunable weak link, Phys. Rev. Lett. **106**, 130401 (2011).

[25] J. Brand and W. P. Reinhardt, Generating ring currents, solitons and svortices by stirring a Bose-Einstein condensate in a toroidal trap, J. Phys. B **34**, L113 (2001).

[26] M. Modugno, C. Tozzo, and F. Dalfovo, Detecting phonons and persistent currents in toroidal Bose-eEinstein condensates by means of pattern formation, Phys. Rev. A **74**, 061601(R) (2006).

[27] S. Beattie, S. Moulder, R. J. Fletcher, and Z. Hadzibabic, Persistent currents in spinor condensates, Phys. Rev. Lett. **110**, 025301 (2013).

[28] A. I. Yakimenko, K. O. Isaieva, S. I. Vilchinskii, and M. Weyrauch, Stability of persistent currents in spinor Bose-Einstein condensates, Phys. Rev. A **88**, 051602(R) (2013).

[29] A. Tononi, L. Salasnich, and A. Yakimenko, Quantum vortices in curved geometries, AVS Quantum Sci. **6**, 030502 (2024).

[30] J. Polo, W. J. Chetcuti, T. Haug, A. Minguzzi, K. Wright, and L. Amico, Persistent currents in ultracold gases, arXiv:2410.17318.

[31] I. Lesanovsky and W. von Klitzing, Spontaneous emergence of angular momentum Josephson oscillations in coupled annular Bose-Einstein condensates, Phys. Rev. Lett. **98**, 050401 (2007).

[32] J. Brand, T. J. Haigh, and U. Zülicke, Rotational fluxons of Bose-Einstein condensates in coplanar double-ring traps, Phys. Rev. A **80**, 011602(R) (2009).

[33] J. Brand, T. J. Haigh, and U. Zülicke, Sign of coupling in barrier-separated Bose-Einstein condensates and stability of double-ring systems, Phys. Rev. A **81**, 025602 (2010).

[34] S.-W. Su, S.-C. Gou, A. Bradley, O. Fialko, and J. Brand, Kibble-zurek scaling and its breakdown for spontaneous generation of Josephson vortices in Bose-Einstein condensates, Phys. Rev. Lett. **110**, 215302 (2013).

[35] M. I. Qadir, H. Susanto, and P. C. Matthews, Fluxon analogues and dark solitons in linearly coupled Bose-Einstein condensates, J. Phys. B **45**, 035004 (2012).

[36] J. Polo, A. Benseny, T. Busch, V. Ahufinger, and J. Mompart, Transport of ultracold atoms between concentric traps via spatial adiabatic passage, New J. Phys. **18**, 015010 (2016).

[37] J. Polo, J. Mompart, and V. Ahufinger, Geometrically induced complex tunnelings for ultracold atoms carrying orbital angular momentum, Phys. Rev. A **93**, 033613 (2016).

[38] S. S. Shamailov and J. Brand, Quasiparticles of widely tuneable inertial mass: The dispersion relation of atomic Josephson vortices and related solitary waves, SciPost Phys. **4**, 018 (2018).

[39] C. Baals, H. Ott, J. Brand, and A. M. N. Mateo, Nonlinear standing waves in an array of coherently coupled Bose-Einstein condensates, Phys. Rev. A **98**, 053603 (2018).

[40] T. W. A. Montgomery, W. Li, and T. M. Fromhold, Spin Josephson vortices in two tunnel-coupled spinor Bose gases, Phys. Rev. Lett. **111**, 105302 (2013).

[41] A. Gallemí, M. Guilleumas, R. Mayol, and A. M. N. Mateo, Multidimensional Josephson vortices in spin-orbit-coupled Bose-Einstein condensates: Snake instability and decay through vortex dipoles, Phys. Rev. A **93**, 033618 (2016).

[42] A. Oliinyk, I. Yatsuta, B. Malomed, and A. Yakimenko, Symmetry breaking in interacting ring-shaped superflows of Bose-Einstein condensates, Symmetry **11**, 1312 (2019).

[43] A. Oliinyk, B. Malomed, and A. Yakimenko, Nonlinear dynamics of Josephson vortices in merging superfluid rings, Commun. Nonlinear Sci. Numer. Simul. **83**, 105113 (2020).

[44] A. Oliinyk, A. Yakimenko, and B. Malomed, Tunneling of persistent currents in coupled ring-shaped Bose-Einstein condensates, J. Phys. B **52**, 225301 (2019).

[45] N. Bazhan, A. Svetlichnyi, D. Pfeiffer, D. Derr, G. Birkl, and A. Yakimenko, Generation of Josephson vortices in stacked toroidal Bose-Einstein condensates, Phys. Rev. A **106**, 043305 (2022).

[46] A. Pérez-Obiol, J. Polo, and L. Amico, Coherent phase slips in coupled matter-wave circuits, Phys. Rev. Res. **4**, L022038 (2022).

[47] D. Hernández-Rajkov, N. Grani, F. Scazza, G. Del Pace, W. Kwon, M. Inguscio, K. Xhani, C. Fort, M. Modugno, F. Marino *et al.*, Connecting shear flow and vortex array instabilities in annular atomic superfluids, Nat. Phys. **20**, 939 (2024).

[48] L. Pezzè, K. Xhani, C. Daix, N. Grani, B. Donelli, F. Scazza, D. Hernandez-Rajkov, W. J. Kwon, G. D. Pace, and G. Roati, Stabilizing persistent currents in an atomtronic Josephson junction necklace, Nat. Commun. **15**, 4831 (2024).

[49] V. M. Kaurov and A. B. Kuklov, Josephson vortex between two atomic Bose-Einstein condensates, Phys. Rev. A **71**, 011601(R) (2005).

[50] V. M. Kaurov and A. B. Kuklov, Atomic Josephson vortices, Phys. Rev. A **73**, 013627 (2006).

[51] L. Amico, G. Birkl, M. Boshier, and L.-C. Kwek, Focus on atomtronics-enabled quantum technologies, New J. Phys. **19**, 020201 (2017).

[52] L. Amico, M. Boshier, G. Birkl, A. Minguzzi, C. Miniatura, L.-C. Kwek, D. Aghamalyan, V. Ahufinger, D. Anderson, N. Andrei *et al.*, Roadmap on atomtronics: State of the art and perspective, AVS Quantum Sci. **3**, 039201 (2021).

[53] A. W. Baggaley and N. G. Parker, Kelvin-Helmholtz instability in a single-component atomic superfluid, Phys. Rev. A **97**, 053608 (2018).

[54] A. Chaika, A. Oliinyk, I. Yatsuta, N. Proukakis, M. Edwards, A. Yakimenko, and T. Bland, Acceleration-induced transport of quantum vortices in joined atomtronic circuits, arXiv:2410.23818.

[55] R. Roy and O. E. Alon, Assessing small accelerations using a bosonic Josephson junction, arXiv:2409.20203.

[56] S. Choi, S. A. Morgan, and K. Burnett, Phenomenological damping in trapped atomic Bose-Einstein condensates, Phys. Rev. A **57**, 4057 (1998).

[57] L. P. Pitaevskii, Phenomenological theory of superfluidity near the λ-point, Zh. Eksp. Teor. Fiz. **35**, 408 (1958) [Sov. Phys. JETP **35**, 282 (1959)].

[58] M. Tsubota, K. Kasamatsu, and M. Ueda, Vortex lattice formation in a rotating Bose-Einstein condensate, Phys. Rev. A **65**, 023603 (2002).

[59] T. Kanai, W. Guo, and M. Tsubota, Merging of rotating bose–einstein condensates, J. Low Temp. Phys. **195**, 37 (2019).

[60] O. Adeniji, C. Henry, S. Thomas, R. C. Sapp, A. Goyal, C. W. Clark, and M. Edwards, Double-target BEC atomtronic rotation sensor, arXiv:2411.06585.

[61] T. Bland, I. V. Yatsuta, M. Edwards, Y. O. Nikolaieva, A. O. Oliinyk, A. I. Yakimenko, and N. P. Proukakis, Persistent current oscillations in a double-ring quantum gas, Phys. Rev. Res. **4**, 043171 (2022).

[62] N. G. Parker, N. P. Proukakis, C. F. Barenghi, and C. S. Adams, Controlled vortex-sound interactions in atomic Bose-Einstein condensates, Phys. Rev. Lett. **92**, 160403 (2004).

[63] C. Qu, M. Tylutki, S. Stringari, and L. P. Pitaevskii, Magnetic solitons in Rabi-coupled Bose-Einstein condensates, Phys. Rev. A **95**, 033614 (2017).

[64] S. Simjanovski, G. Gauthier, M. J. Davis, H. Rubinsztein-Dunlop, and T. W. Neely, Optimizing persistent currents in a ring-shaped Bose-Einstein condensate using machine learning, Phys. Rev. A **108**, 063306 (2023).

[65] G. Del Pace, K. Xhani, A. Muzi Falconi, M. Fedrizzi, N. Grani, D. Hernandez Rajkov, M. Inguscio, F. Scazza, W. J. Kwon, and G. Roati, Imprinting persistent currents in tunable fermionic rings, Phys. Rev. X **12**, 041037 (2022).